Emergent superconductivity in two-dimensional NiTe$_2$ crystals

Feipeng Zheng [1,*] Xi-Bo Li,[1] Peng Tan,[1] Yiping Lin,[1] Lingxiao Xiong,[1] Xiaobo Chen,[1] and Ji Feng [2,3,†]

[1] *Siyuan Laboratory, Guangzhou Key Laboratory of Vacuum Coating Technologies and New Energy Materials,*
Department of Physics, Jinan University, Guangzhou 510632, China
[2] *International Center for Quantum Materials, School of Physics, Peking University, Beijing 100871, China*
[3] *Collaborative Innovation Center of Quantum Matter, Beijing 100871, China*

Two-dimensional superconductors exfoliated from layered materials harbor novel superconductivity and exotic correlated phases, often concomitantly, but their discovery has been few and far between. Employing the anisotropic Migdal-Eliashberg formalism based on *ab initio* calculations, we find monolayer NiTe$_2$ to be an intrinsic superconductor with a $T_c \sim 5.7$ K, although the bulk crystal is not known to superconduct. Remarkably, bilayer NiTe$_2$ intercalated with lithium is found to display two-gap superconductivity with a critical temperature $T_c \sim 11.3$ K and a superconducting gap of ~ 3.1 meV, arising from a synergy of electronic and phononic effects. As monolayer and bilayer NiTe$_2$ have been recently isolated experimentally, and lithium can be inserted into the bilayer via ionic liquid gating, the comparatively high T_c, substrate independence, and proximity tunability will make these superconductors ideal platforms for exploring intriguing correlation effects and quantum criticality associated two-dimensional superconductivity.

Highly crystalline two-dimensional superconductors derived from exfoliated layered materials represent a unique class of two-dimensional superconductivity without the need for an indispensable substrate [1–8]. In spite of the fascinating physics associated with them, the discovery of these exfoliated two-dimensional superconductors has been few and far between [3–7]. In particular, monolayer transition metal dichalcogenides, NbSe$_2$ and TaS$_2$, thinned down to the monolayer limit display coexisting superconductivity and charge-density wave driven by electron-phonon coupling [1,7,9–11]. These two-dimensional crystals can be transferred from one substrate to another, and the superconductivity persists subject to perhaps mild tuning by the substrate in proximity. Thus, this class of highly crystalline superconductors harbors truly two-dimensional and freestanding superconductivity, offering an ideal platform for exploring the interplay of novel superconductivity, quantum criticality, and electron correlation effects, as well as novel superconducting device systems [1–3,5–12].

Indeed, the aforementioned NbSe$_2$ and TaS$_2$ in its bulk crystalline form are archetypical layered transition metal dichalcogenides, both of which undergo a phase transition to a commensurate charge-density wave phase and then another into an anisotropic s-wave superconductors at the superconducting transition temperature T_c. And they are about the only known examples of intrinsic two-dimensional superconductors exfoliated from layered transition metal dichalcogenides. Clearly, the availability of superconducting phase in the true two-dimensional limit will help shed light on the decades-old puzzle regarding the coexistence and interplay of these competing orders [1], in addition to the exploration of novel physics in two-dimensional superconducting phases. There also appears to be an *imminent* spin-density wave when NbSe$_2$ is thinned to monolayer limit in addition to the coexistent superconductivity and charge-density wave [10,11], which may be suggesting a highly curious possibility that two-dimensional crystalline superconductors may have a phase diagram resembling those in the high-T_c class. The lack of such materials hinders the exploration of such phase diagrams. Therefore, it is highly desirable to find more examples of two-dimensional crystalline superconductors, to bring forth such an intriguing possibility while examining all the aforementioned fascinating physics.

This Rapid Communication reports a computational investigation of the superconductivity in two-dimensional crystals of a transition metal dichalcogenide NiTe$_2$, where the superconducting temperature is calculated based on the anisotropic Midgal-Eliashberg formalism. Recently, NiTe$_2$ two-dimensional crystals have been successfully prepared with an accurate number of layers down to monolayer limit [13]. Although the bulk NiTe$_2$ is not known to superconduct, we find that a two-gap superconductivity emerges in the monolayer limit, with a $T_c \sim 5.7$ K. We show that Li-intercalated bilayer NiTe$_2$ tends to form the structure where all the intercalated sites are occupied by Li. Surprisingly, the superconductivity disappears in a bilayer geometry, but when the bilayer NiTe$_2$ is intercalated with alkali metals a two-gap superconductor reemerges with T_c as high as 11.3 K and a superconducting gap up to 3.1 meV. The superconducting mechanism and effects of Li intercalation are analyzed in detail. The T_c can be further enhanced by in-plane

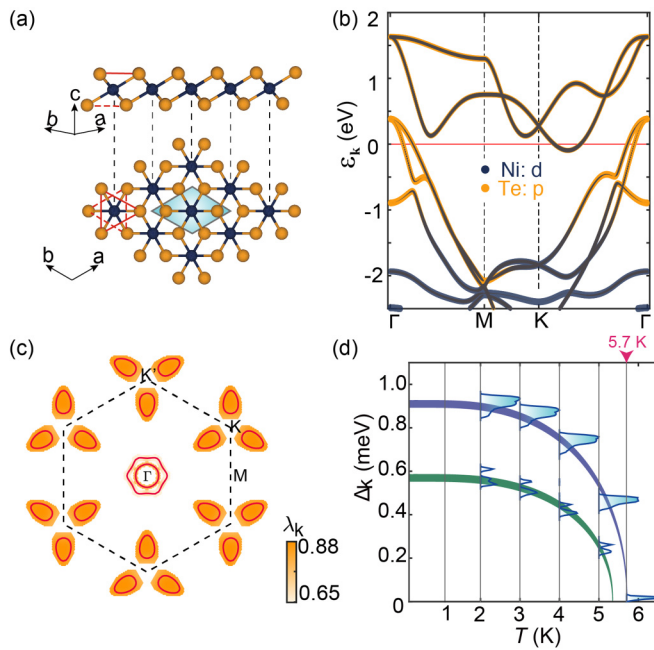*fpzheng_phy@jnu.edu.cn
†jfeng11@pku.edu.cn

FIG. 1. (a) Side (top) and top (bottom) views of the crystal structure of monolayer $NiTe_2$. The filled rhombus corresponds to a primitive unit cell. (b) Band structure with projections onto constituent atoms, and (c) Fermi surface (red lines) of the monolayer superimposed with the distribution of λ_k around the Fermi surface. (d) Histograms of $\Delta_k(\omega)$, evaluated at T's from 2 to 6 K. The blue and green curves are BCS fits.

compressive strain and electron doping, suggesting the substrate with smaller lattice constant and higher work function can help to promote the T_c of monolayer $NiTe_2$.

In a single-layer $NiTe_2$, each Ni atom is situated in the center of an octahedral cage formed by Te as shown in Fig. 1(a). Te atoms occupy vertices of trigonally squashed octahedra, which then share edges to inflate into a two-dimensional sheet, with the $1T$-type structure. Multilayer $NiTe_2$ and bulk crystals are composed of AA stacked monolayers. It is noted that the interlayer gallery of $NiTe_2$ has a spacing of 2.63 Å, which is considerably smaller than other transition metal dichalcogenides (e.g., 3.08 Å for $TiTe_2$, 2.89 Å for WTe_2, 2.90 Å for $NbSe_2$), indicating relatively strong interlayer coupling. Density-functional theory and density-functional perturbation theory calculations are performed to study the crystal, electronic, and phonon structures and the electron-phonon coupling of few-layer $NiTe_2$ [14–17]. The Kohn-Sham valence states on an 18×18 k grid are expanded as plane waves below 100 Rydberg, whereupon the geometric and electronic structures are evaluated.

The optimized structure of bulk $NiTe_2$ using different types of exchange-correlation functionals are carefully examined. We found that both the standard generalized-gradient Perdew-Burke-Ernzerhof (PBE) functional [17], and the PBE incorporating long-range van der Waals interaction [18,19] predict lattice constants sufficiently close to the experiments [20–22]. The optimized a value for monolayer $NiTe_2$ is 3.772 Å, which is smaller than bulk, but becomes very close to the bulk value for multilayer $NiTe_2$.

We begin by highlighting the main features of the electronic and phonon band structures in monolayer $NiTe_2$. Figures 1(b) and 1(c) display the projected band structure and Fermi surface: three bands across Fermi level, ε_F, which makes the monolayer a compensated metal, as shown in Fig. 1(b). There are two hole pockets at Γ, ascribable mainly to the p orbitals on Te. At the corners of the Brillouin zone, K and K', are clover-shaped electron pockets with three separate petals each [Fig. 1(c)], which are an admixture of d orbitals of Ni and p orbitals of Te [Fig. 1(b)]. The phonon spectrum shows [22] no soft modes, indicating the stability of the optimized crystal structure, especially against charge-density waves. The projected phonon density of states [22] reveals that the optical phonons are segregated into two rather narrow sectors with a 12-meV gap between them, featuring, respectively, Te-dominated modes at 10–16 meV and Ni-dominated modes at 28–30 meV.

In order to assess the superconductivity of monolayer $NiTe_2$, we employ the imaginary-time anisotropic Migdal-Eliashberg formalism [23,24] with subsequent analytic continuation to the real axis using Padé functions, which provides a quantitatively adequate description of electron-phonon coupling driven superconductivity in layered crystals [25,26], with which the superconducting gap $\Delta(\boldsymbol{k}, \omega)$ is obtained by solving [26,27] the gap equation at finite temperatures. Only the Kohn-Sham states within 100 meV of ε_F are included, and the Matsubara frequencies are cut off at 0.32 eV. Electron-phonon coupling matrix elements are first computed on the above $\boldsymbol{k}$ and $\boldsymbol{q}$ grids, then interpolated [28] to grids of 120×120. The Coulomb pseudopotential μ^* is estimated to be 0.17 according to $\mu^* \approx \{0.26N(0)/[1 + N(0)]\}$ [29], where $N(0)$ is the electronic density of states at ε_F.

The Migdal-Eliashberg equations are then solved at finite temperatures for the superconducting gap $\Delta(\boldsymbol{k}, \omega)$ [30] whereupon the T_c is determined. The $\boldsymbol{k}$-resolved superconducting gap on the Fermi surface, $\Delta_k(T)$, for temperatures between 2 and 6 K and $\omega = 0$, are displayed in Fig. 1(d). It is seen that the gap vanishes at around 5.7 K, already higher than the liquid-helium temperature. Below the transition temperature, we see that the superconductivity shows a patent two-gap feature, a point to be returned to shortly. It is worth remarking that the T_c obtained with the McMillan-Allen-Dynes (MAD) approach [30–32], which assumes an isotropic spectrum, is around 2.3 K for the monolayer. Solving the full Midgal-Eliashberg gap equation is evidently more reliable given the reduced dimensionality and anisotropic Fermi surface [25,26,33]. It is also noted that the superconducting transition T_c computed using MAD and Migdal-Eliashberg approaches for bulk $NiTe_2$ are both very close to zero temperature, consistent with the fact that bulk $NiTe_2$ has not been reported to superconduct. The in-plane compressive strain and electron doping can further enchance the T_c of the monolayer [22].

Interestingly, our calculations also show that the estimated T_c's using both the MAD and Midgal-Eliashberg of bilayer $NiTe_2$ are below 1 K [22]. This and the absence of superconductivity in bulk $NiTe_2$ possibly indicate that the reduced interlayer spacing and concomitant strong interlayer coupling, as mentioned earlier, in this layered material is detrimental to superconductivity (see Sec. S10 of the Supplemental Material
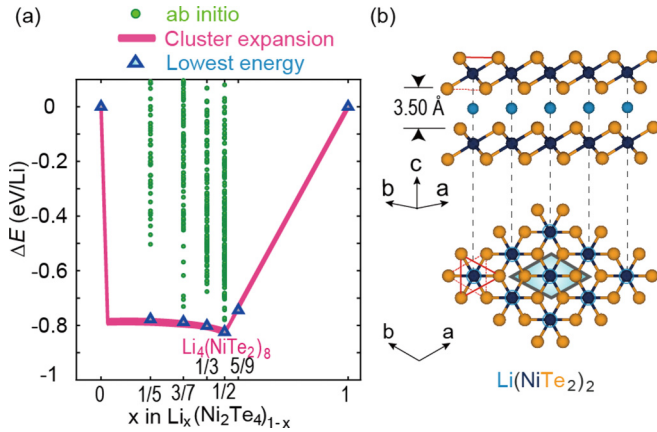
FIG. 2. (a) Computed formation energies for $Li_x(Ni_2Te_4)_{1-x}$. The green dots are the energies of structures sampled by an *ab initio* method (DFT), with blue triangles indicating the lowest-energy structures. The magenta outline is the convex hull from cluster expansion. (b) Side view (upper) and top view (lower) of the crystal structure of $LiNi_2Te_4$. The light-blue circles indicate intercalation sites.

[22]). This observation naturally begets the question whether the superconductivity seen in monolayer can be reconstituted if we can weaken the interlayer coupling by, for example, augmenting interlayer spacing. Indeed, the interlayer space of layered structures is a natural gallery for a wide range of chemical species, through a chemical process called intercalation whereupon the interlayer space gets expanded by the intercalant [34]. Here, we choose a family of simplest atomic intercalant, alkali metals, which can be inserted into few-layer $NiTe_2$ via ionic liquid gating. We shall focus mostly on lithium insertion in the following discussion, as it produces the most dramatic boost to the superconducting T_c [22].

The energetically most favored lithium-intercalated $NiTe_2$ bilayer has a stoichiometry, $LiNi_2Te_4$, of which the structure is displayed in Fig. 2(b). Li atoms are located precisely in between two eclipsed Ni from the two monolayers, forming a two-dimensional hexagonal lattice. The stoichiometry and structure are arrived at from the zero-temperature formation energies computed for a total of 36 200 candidate lithium intercalation structures at multiple stoichiometries, combining *ab initio* particle-swarm optimization [35] and random sampling of structures using a Hamiltonian based on cluster expansion [22]. The resultant convex hull of formation energy of lithium-intercalated bilayer $NiTe_2$ is shown in Fig. 2(a), pointing to the aforementioned stoichiometry and structure as thermodynamically stable against decomposition to any other stoichiometry. The interlayer gallery in $LiNi_2Te_4$ is substantially expanded to 3.50 Å, as compared to 2.67 Å in the pristine bilayer.

The low-energy electronic excitations of $LiNi_2Te_4$ bears essential similarity with the pristine monolayer $NiTe_2$, but with a few remarkable departures. As shown in Fig. 3(a), the tortuous t_{2g}-e_g gap is by and large preserved, although there is a substantial electron doping into the $NiTe_2$'s e_g bands, the bottom of which also hybridize with lithium orbitals. Due to electron transfer from Li, large hole pockets entering M and Γ points emerge, showing simultaneous Ni, Te, and Li
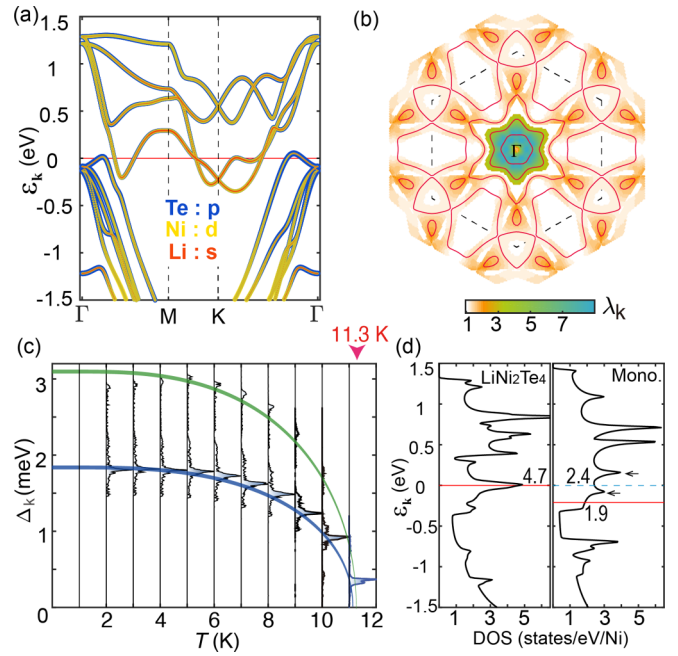

FIG. 3. (a) The band structure with projections onto constituent atoms and (b) Fermi surfaces (red lines) for $LiNi_2Te_4$, superimposed with λ_k around the Fermi surface. (c) Histograms of Δ_k of Ni_2LiTe_4 at various temperatures. Blue and green curves are BCS fits of the two gaps. (d) Electronic density of states of $LiNi_2Te_4$ (left) and monolayer $NiTe_2$ (right). The solid red lines indicate Fermi levels.

hybridization. The p-d hybridized electron pockets at K and K' are also slightly enlarged and three petals become fused at a pistil, as shown in Fig. 3(b). The t_{2g} bands show splittings owing to interlayer coupling mediated by the intercalated lithium, whereas the hole pockets at Γ are still dominated by p orbitals of Te.

Remarkably, superconductivity computed to disappear in the pristine bilayer reappears in the lithium-intercalated bilayer with a significant boost. The Migdal-Eliashberg formalism leads to a T_c above 11.3 K, which is significantly higher than the transition temperatures of monolayer and bilayer $NiTe_2$. The histograms of Δ_k for temperatures between 2 and 12 K are displayed in Fig. 3(c), which again shows clearly two temperature-dependent gaps. The BCS fits for the two gaps are also plotted as solid lines in green and blue, respectively. Both of the gaps decrease with rising temperature, with a T_c of 11.1 and 11.3 K, respectively. The zero-temperature superconducting gaps are, respectively, 3.1 and 1.8 meV, both significantly higher than the monolayer counterparts. The conspicuously boosted T_c in $LiNi_2Te_4$ suggests that the intercalated Li plays decisive roles in the emerging superconductivity, which is to be clarified next.

There is a significant electronic modification in the bilayer $NiTe_2$ intercalated with lithium. As seen in Fig. 3(d), $LiNi_2Te_4$ has a Fermi density of states $N(0) = 4.7$ per eV (density of states is given on a per Ni basis), enjoying a near 2.5-fold increase over that of the pristine monolayer $NiTe_2$, where $N(0) = 1.9$ per eV. The intercalated lithiums donate nominally one electron per atom to the $NiTe_2$ bilayer. But doping alone is insufficient to produce a boost in the Fermi density
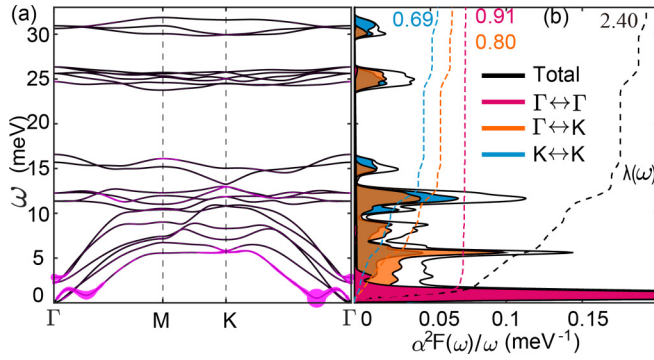
FIG. 4. (a) Computed phonon dispersion $\omega_{\mathbf{q}\nu}$ of LiNi$_2$Te$_4$, superimposed with $\lambda_{\mathbf{q}\nu}$, which is positively correlated to the size of the pink dot. (b) Total and partial mass-enhancement parameter $\gamma(P \leftrightarrow Q, \omega) = \alpha^2 F(P \leftrightarrow Q, \omega)/\omega$, where $(P, Q = \Gamma, K)$ (see main text). The corresponding accumulated electron-phonon coupling constants $\lambda(P \leftrightarrow Q, \omega)$ are depicted using colored dashed lines.

of states. It can be seen from Fig. 3(d) that adding a half electron to the pristine monolayer increases $N(0)$ to a meager 2.4 per eV. The sharp peak at Fermi level in LiNi$_2$Te$_4$ is brought about by Van Hove singularities along the Γ-K path, as shown in Fig. 3(a), which results from lithium-mediated interlayer coupling. The increased density of states on the Fermi level means more electrons are susceptible to pairing interaction maybe mediated by dynamical phonons, which certainly contributes to the increased T_c.

On top of multiplying the conducting electrons, the intercalated lithium also significantly enhances the electron-phonon coupling. This can be seen from the overall mass-enhancement factor of LiNi$_2$Te$_4$, $\lambda = 2.4$ as shown in Fig. 4(b), which is more than threefold escalation from the pristine monolayer where $\lambda = 0.74$. In the meantime, the presence of lithium, by virtue of its light mass and therefore large dynamical scale, gives rise to energetic phonons at around 31 meV [22]. This leads to an increase in $\omega_{\log}$ by $\sim 10\%$. Thus, even in the isotropic MAD estimate, an increase in the superconducting T_c is expected. Indeed, the MAD approach gives a $T_c \sim 4.8$ K [22], which is an inadequate estimate as the spectrum is evidently anisotropic.

A more detailed view of the electron-phonon coupling in the superconducting LiNi$_2$Te$_4$ can be gained by inspecting the $\mathbf{k}$-resolved mass-enhancement factor,

$$\lambda_{\mathbf{k}} = \frac{1}{N(0)} \int \frac{d\omega}{\omega} \sum_{\mathbf{k}'} \alpha^2 F(\mathbf{k}, \mathbf{k}', \omega) \delta(\epsilon_{\mathbf{k}'}), \qquad (1)$$

where ω is phonon frequency, α^2 the electron-phonon coupling strength averaged over the Fermi surface, and $F(\mathbf{q}, \omega)$ the phonon spectral function. The values of $\lambda_{\mathbf{k}}$ in the vicinity of Fermi surfaces are shown in Fig. 1(c) for monolayer NiTe$_2$ and in Fig. 3(b) for LiNi$_2$Te$_4$. This Migdal spectroscopy reveals a pervading enhancement of electron-phonon coupling in LiNi$_2$Te$_4$ in comparison with monolayer NiTe$_2$; that is, the dimensionless $\lambda_{\mathbf{k}}$ takes generally larger values in the former. In particular, the hole pockets centered at Γ of the electron-phonon coupling experience the strongest electron-phonon coupling, which arises from scattering with phonons in the low-energy regime, as seen in Fig. 4(b), where

there is a sharp peak of partial mass-enhancement parameter $\gamma(\Gamma \leftrightarrow \Gamma)$. Here, $\gamma(P \leftrightarrow Q)$ is obtained by integrating $\alpha^2 F(\mathbf{k}, \mathbf{k}', \omega)/\omega$, restricting the momenta $\mathbf{k}$ to the P pocket and $\mathbf{k}'$ to the Q pocket [cf. Eq. (1) and see Sec. S2 of the Supplemental Material [22]]. These softened optical modes along the Γ-K path indicate an imminent charge-density wave, which makes the low-frequency phonons scatter strongly the holes near Γ, leading to large $\lambda_{\mathbf{k}}$ in this region. We further find that the charge-density wave may be induced by in-plane tensile strain, suggesting a possible coexistence of charge-density wave and superconductivity which needs further investigation.

In summary, using *ab initio* calculation based on anisotropic Migdal-Eliashberg theory within the static lattice approximation, we have shown the emergence of two-gap superconductivity in two-dimensional NiTe$_2$ crystals, namely, monolayer NiTe$_2$ and lithium-intercalated bilayer, although the bulk NiTe$_2$ does not superconduct. The energetically most favored lithium-intercalated bilayer, LiNi$_2$Te$_4$, is computed to have a relatively high superconducting transition T_c up to 11.3 K with superconducting gaps up to 3.1 meV, whereas the monolayer has a T_c of 5.7 K and the pristine bilayer NiTe$_2$ is nonsuperconducting. The T_c of the Li-interacalted bilayer is highest among all known phonon-mediated two-dimensional superconductors exfoliated from layered materials [1,7], and among layered materials, it is only second to MgB$_2$ [25] and on a par with Ca-intercalated graphite [36]. The remarkable enhancement of superconductivity in the lithium-intercalated bilayer is attributable to the synergy of electron doping and lithium-mediated interlayer hybridization and the accompanying electron-phonon coupling, as well as energetic phonons due to the intercalated lithium. It should be remarked that given the exceedingly strong coupling between the lattice and electron in the Li-intercalated bilayer, the normal state may become a non-Fermi liquid, which is not captured in the current theoretical framework but will be a highly intriguing scenario for further investigation.

Finally, remarks on the experimental preparation of these emergent highly crystalline two-dimensional superconductors are in order. The NiTe$_2$ monolayer and bilayer have already been experimentally synthesized [13], and their superconductivity and the absence thereof can be straightforwardly probed. The lithium intercalation to the bilayer can be achieved with ionic liquid gating [37–40]. Therefore, the experimental accessibility, combined with the relatively high T_c, substrate independence, and proximity tunability will make these superconductors ideal platforms for exploring intriguing correlation effects and quantum criticality associated two-dimensional superconductivity. We have also examined the intercalation of bilayer NiTe$_2$ with sodium and potassium, with corresponding $T_c = 4.4$ and 3.1 K, respectively [22], which are also interesting possibilities worth experimental assaying.

[1] M. M. Ugeda, A. J. Bradley, Y. Zhang, S. Onishi, Y. Chen, W. Ruan, C. Ojeda-Aristizabal, H. Ryu, M. T. Edmonds, H.-Z. Tsai, A. Riss, S.-K. Mo, D. Lee, A. Zettl, Z. Hussain, Z.-X. Shen, and M. F. Crommie, Nat. Phys. **12**, 92 (2015).

[2] Y. Cao, V. Fatemi, S. Fang, K. Watanabe, T. Taniguchi, E. Kaxiras, and P. Jarillo-Herrero, Nature (London) **556**, 43 (2018).

[3] D. Jiang, T. Hu, L. You, Q. Li, A. Li, H. Wang, G. Mu, Z. Chen, H. Zhang, G. Yu, J. Zhu, Q. Sun, C. Lin, H. Xiao, X. Xie, and M. Jiang, Nat. Commun. **5**, 5708 (2014).

[4] Y. Yu, L. Ma, P. Cai, R. Zhong, C. Ye, J. Shen, G. D. Gu, X. Chen, and Y. Zhang, Nature (London) **575**, 156 (2019).

[5] X. Xi, L. Zhao, Z. Wang, H. Berger, L. Forró, J. Shan, and K. F. Mak, Nat. Nanotechnol. **10**, 765 (2015).

[6] Y. Cao, A. Mishchenko, G. L. Yu, E. Khestanova, A. P. Rooney, E. Prestat, A. V. Kretinin, P. Blake, M. B. Shalom, C. Woods, J. Chapman *et al.*, Nano Lett. **15**, 4914 (2015).

[7] E. Navarro-Moratalla, J. O. Island, S. Manñs-Valero, E. Pinilla-Cienfuegos, A. Castellanos-Gomez, J. Quereda, G. Rubio-Bollinger, L. Chirolli, J. A. Silva-Guillén, N. Agraït, G. A. Steele, F. Guinea, H. S. J. Van Der Zant, and E. Coronado, Nat. Commun. **7**, 11043 (2016).

[8] Z.-Y. Cao, J.-W. Hu, A. F. Goncharov, and X.-J. Chen, Phys. Rev. B **97**, 214519 (2018).

[9] X. Xi, Z. Wang, W. Zhao, J.-H. Park, K. T. Law, H. Berger, L. Forró, J. Shan, and K. F. Mak, Nat. Phys. **12**, 139 (2015).

[10] F. Zheng, Z. Zhou, X. Liu, and J. Feng, Phys. Rev. B **97**, 081101(R) (2018).

[11] F. Zheng and J. Feng, Phys. Rev. B **99**, 161119(R) (2019).

[12] H. Wang, X. Huang, J. Lin, J. Cui, Y. Chen, C. Zhu, F. Liu, Q. Zeng, J. Zhou, P. Yu *et al.*, Nat. Commun. **8**, 394 (2017).

[13] B. Zhao, W. Dang, Y. Liu, B. Li, J. Li, J. Luo, Z. Zhang, R. Wu, H. Ma, and G. Sun, J. Am. Chem. Soc. **140**, 14217 (2018).

[14] S. Baroni, P. Giannozzi, and A. Testa, Phys. Rev. Lett. **58**, 1861 (1987).

[15] P. Giannozzi, S. Baroni, N. Bonini, M. Calandra, R. Car, C. Cavazzoni, D. Ceresoli, G. L. Chiarotti, M. Cococcioni, I. Dabo *et al.*, J. Phys.: Condens. Matter **21**, 395502 (2009).

[16] D. R. Hamann, M. Schlüter, and C. Chiang, Phys. Rev. Lett. **43**, 1494 (1979).

[17] J. P. Perdew, K. Burke, and M. Ernzerhof, Phys. Rev. Lett. **77**, 3865 (1996).

[18] I. Hamada, Phys. Rev. B **89**, 121103(R) (2014).

[19] K. Lee, É. D. Murray, L. Kong, B. I. Lundqvist, and D. C. Langreth, Phys. Rev. B **82**, 081101(R) (2010).

[20] W. Bensch, W. Heid, M. Muhler, S. Jobic, R. Brec, and J. Rouxel, J. Solid State Chem. **121**, 87 (1996).

[21] S. Furuseth, K. Selte, and A. Kjekshus, Acta Chem. Scand. **19**, 257 (1965).

[22] See Supplemental Material at http://link.aps.org/supplemental/10.1103/PhysRevB.101.100505 for details of computational methods, phonons and mass-enhancement factor in monolayer NiTe$_2$, computed electron-phonon coupling properties of bulk and bilayer NiTe$_2$, strain engineering on the electron-phonon coupling of monolayer NiTe$_2$, partial phonon density of states of LiNi$_2$Te$_4$, comparison of computed superconducting properties of LiNi$_2$Te$_4$ using different exchange-correlation functionals, and enhanced electron-phonon coupling in NaNi$_2$Te$_4$ and KNi$_2$Te$_4$.

[23] A. B. Migdal, Zh. Eksp. Teor. Fiz. **34**, 1438 (1960) [Sov. Phys. JETP **34**, 996 (1958)].

[24] G. M. Eliashberg, Zh. Eksp. Teor. Fiz. **38**, 966 (1960) [Sov. Phys. JETP **11**, 696 (1960)].

[25] H. J. Choi, D. Roundy, H. Sun, M. L. Cohen, and S. G. Louie, Nature (London) **418**, 758 (2002).

[26] E. R. Margine and F. Giustino, Phys. Rev. B **87**, 024505 (2013).

[27] S. Poncé, E. R. Margine, C. Verdi, and F. Giustino, Comput. Phys. Commun. **209**, 116 (2016).

[28] A. A. Mostofi, J. R. Yates, Y.-S. Lee, I. Souza, D. Vanderbilt, and N. Marzari, Comput. Phys. Commun. **178**, 685 (2008).

[29] K. H. Bennemann and J. W. Garland, *Theory for Superconductivity in d-Band Metals* AIP Conf. Proc. No. 4 (AIP, New York, 1972), p. 103.

[30] F. Giustino, Rev. Mod. Phys. **89**, 015003 (2017).

[31] W. L. McMillan, Phys. Rev. **167**, 331 (1968).

[32] P. B. Allen and R. C. Dynes, Phys. Rev. B **12**, 905 (1975).

[33] A. Sanna, S. Pittalis, J. K. Dewhurst, M. Monni, S. Sharma, G. Ummarino, S. Massidda, and E. K. U. Gross, Phys. Rev. B **85**, 184514 (2012).

[34] *Physics of Intercalation Compounds*, edited by L. Pietronero and E. Tosatti (Springer, New York, 1981).

[35] Y. Wang, J. Lv, L. Zhu, and Y. Ma, Phys. Rev. B **82**, 094116 (2010).

[36] T. E. Weller, M. Ellerby, S. S. Saxena, R. P. Smith, and N. T. Skipper, Nat. Phys. **1**, 39 (2005).

[37] P. C. Klipstein, C. M. Pereira, and R. H. Friend, Philos. Mag. B **56**, 531 (1987).

[38] Y. Yu, F. Yang, X. Lu, Y. Yan, Y.-H. Cho, L. Ma, X. Niu, S. Kim, Y.-W. Son, D. Feng *et al.*, Nat. Nanotechnol. **10**, 270 (2015).

[39] E. Sajadi, T. Palomaki, Z. Fei, W. Zhao, P. Bement, C. Olsen, S. Luescher, X. Xu, J. Folk, and D. H. Cobden, Science **362**, 922 (2018).

[40] V. Fatemi, S. Wu, Y. Cao, L. Bretheau, Q. Gibson, K. Watanabe, T. Taniguchi, R. Cava, and P. Jarillo-Herrero, Science **362**, 926 (2018).